Inorg. Chem. **2008**, *47*, 11950−11957

Controlled Solvothermal Synthesis of Nanosheets, Nanobelts, and Ultralong Nanobelt Arrays with Honeycomb-Like Micropatterns of ZnSe on Zinc Substrate

Lihui Zhang,[†] Heqing Yang,[*,†] Li Li,[†] Ruigang Zhang,[†] Ruini Liu,[†] Junhu Ma,[†] Xiaoli Xie,[†] and Fei Gao[‡]

Key Laboratory of Macromolecular Science of Shaanxi Province, School of Chemistry and Materials Science, and School of Physics & Information Technology, Shaanxi Normal University, Xi'an 710062, China

Received June 8, 2008

Nanosheets, nanobelts, and ultralong nanobelt arrays with honeycomb-like micropatterns of ZnSe were synthesized via a solvothermal reaction of Zn with Se and KBH_4 in ethylenediamine at 200 °C for 24 h and subsequent annealing. The control over these nanostructures with different morphologies was achieved by adjusting the KBH_4/Se molar ratio. The role of KBH_4 in the formation of $ZnSe(en)_{0.5}$ nanobelts with different length-to-width ratios was investigated, and a possible mechanism was also proposed to account for the growth and conversion of these precursor nanostructures into ZnSe nanostructures. Current−voltage behaviors of the ultralong nanobelt arrays with honeycomb-like micropatterns were investigated. In addition, variable-aspect ratio ZnS nanosheets and nanowires were also synthesized by adjusting the KBH_4/thiourea molar ratio in the Zn−thiourea−KBH_4−ethylenediamine solvothermal system. The results suggest that this method may be employed for the controllable synthesis of other II−VI semiconductor nanostructures such as ZnTe, NiS, MnS, and so forth and provides opportunities for both fundamental research and technological applications.

1. Introduction

Semiconductor nanocrystals with a defined size and shape have drawn much attention in recent years because of their great potential for fundamental research on the effect of dimensionality and size on physical and chemical properties, as well as for electronic and optoelectronic nanodevice applications.[1] Zinc selenide (ZnSe), an important II−VI semiconductor, has been considered as a perspective material for optoelectronic devices, including blue laser diodes, light-emitting diodes, and photodetectors, due to its wide direct band gap (2.67 eV) and large exciton binding energy (21 meV) and so forth.[2−4] Moreover, ZnSe is also a promising material for windows, lenses, output couplers, beam expanders, and optically controlled switching due to its low absorptivity at infrared wavelengths, its visible transmission, and its giant photosensitivity.[5] Recently, various physical and chemical routes such as thermal evaporation, chemical vapor deposition (CVD), laser ablation (LA), molecular beam epitaxy (MBE), metal-organic chemical vapor deposition (MOCVD), and wet chemical synthesis have been employed to prepare ZnSe nanostructured materials in various geometrical morphologies, including zero-dimensional (0D) nanoparticles;[6] one-dimensional (1D) nanorods,[7] nanowires,[8]

* Author to whom correspondence should be addressed. Fax: +86-29-85307774. E-mail: hqyang@snnu.edu.cn.
† School of Chemistry and Materials Science.
‡ School of Physics & Information Technology.

(1) Duan, X. F.; Huang, Y.; Cui, Y.; Wang, J.; Lieber, C. M. *Nature* **2001**, *409*, 66.
(2) Xiong, S. L.; Shen, J. M.; Xie, Q.; Gao, Y. Q.; Tang, Q.; Qian, Y. T. *Adv. Funct. Mater.* **2005**, *15*, 1787.
(3) Xiang, B.; Zang, H. Z.; Li, G. H.; Yang, F. H.; Su, F. H.; Wang, R. M.; Xu, J.; Lu, G. W.; Sun, X. C.; Zhao, Q.; Yu, D. P. *Appl. Phys. Lett.* **2003**, *82*, 3330.
(4) Wang, C. R.; Wang, J.; Li, Q.; Yi, G. C. *Adv. Funct. Mater.* **2005**, *15*, 1471.
(5) Tafreshi, M. J.; Balakrishna, K.; Dhansekaran, R. *J. Mater. Sci.* **1997**, *32*, 3517.
(6) (a) Wang, W. Z.; Geng, Y.; Yan, P.; Liu, F. Y.; Xie, Y.; Qian, Y. T. *J. Am. Chem. Soc.* **1999**, *121*, 4062. (b) Li, Y. D.; Ding, Y.; Qian, Y. T.; Zhang, Y.; Yang, L. *Inorg. Chem.* **1998**, *37*, 2844.
(7) (a) Yang, J.; Xue, C.; Yu, S. H.; Zeng, J. H.; Qian, Y. T. *Angew. Chem.* **2002**, *114*, 4891. (b) Panda, A. B.; Glaspell, G.; El-Shall, M. S. *J. Am. Chem. Soc.* **2006**, *128*, 2790.
(8) (a) Zhang, X. T.; Liu, Z.; Leung, Y. P.; Li, Q.; Hark, S. K. *Appl. Phys. Lett.* **2003**, *83*, 5533. (b) Zhu, Y. C.; Bando, Y. S. *Chem. Phys. Lett.* **2003**, *377*, 367.

10.1021/ic801054e CCC: $40.75
Published on Web 11/08/2008

nanobelts,[9] nanoneedles,[10] nanosaws, and nanotubes;[11] two-dimensional (2D) nanoplates;[12] and three-dimensional (3D) complicated hierarchical nanostructures.[13,14] Up to now, most of this research has focused on ZnSe 0D nanoparticles and 1D nanostructures. In contrast, the investigations on 2D nanostructures, 3D hierarchical structures, and the controlled growth of ZnSe nanostructures with different morphologies are quite rare.[2] Hierarchical assembly of nanoscale building blocks (nanoparticles, nanowires, nanotubes, and nanosheets) is a crucial step toward the realization of functional nanosystems and represents a significant challenge in the field of nanoscale science.[15] Recently, ZnSe hollow microspheres assembled with nanoparticles[13] and ZnSe nanowire bundles,[2] and flowerlike patterns of radically aligned ZnSe nanoflakes[14] have been synthesized. However, to our knowledge, there are no reports about ultralong ZnSe nanobelt arrays with honeycomb-like micropatterns, and no technique has been realized for the controlled synthesis of 1D and 2D nanosized ZnSe building blocks and 3D ZnSe superstructures.

Among these processes for the synthesis of ZnSe nanostructures, the gas-phase approaches (CVD, LA, MBE, and MOCVD) generally require highly sophisticated equipment, toxic metalorganic compounds, and elevated temperatures of 450−1000 °C, and they often face other limitations in terms of sample uniformity and low product yield. The solution approaches to ZnSe nanostructures are appealing because of their low growth temperatures and good potential for scaleup. Herein, we report a novel and very simple approach for the controlled synthesis of nanosheets, nanobelts, and ultralong nanobelt arrays with honeycomb-like micropatterns of ZnSe. These ZnSe nanostructures were synthesized via a solvothermal reaction of Zn with Se and KBH_4 in ethylenediamine (en) and subsequent annealing, and their control was achieved by adjusting the KBH_4/Se molar ratio. Current−voltage (I−V) behaviors of the ultralong nanobelt arrays with honeycomb-like micropatterns were investigated, and the formation mechanism of these nanostructures was also discussed.

2. Experimental Section

All reagents used were of analytical purity and were used directly without further purification. Zn foils (99.99%) and absolute ethanol were from the Xi'an chemical reagent factory, China. Se (99.95%), en, KBH_4, and $NaBH_4$ were from the Beijing chemical reagent factory, China. Zinc foils were polished with sandpaper, ultrasonically washed in absolute ethanol, and then dried naturally.

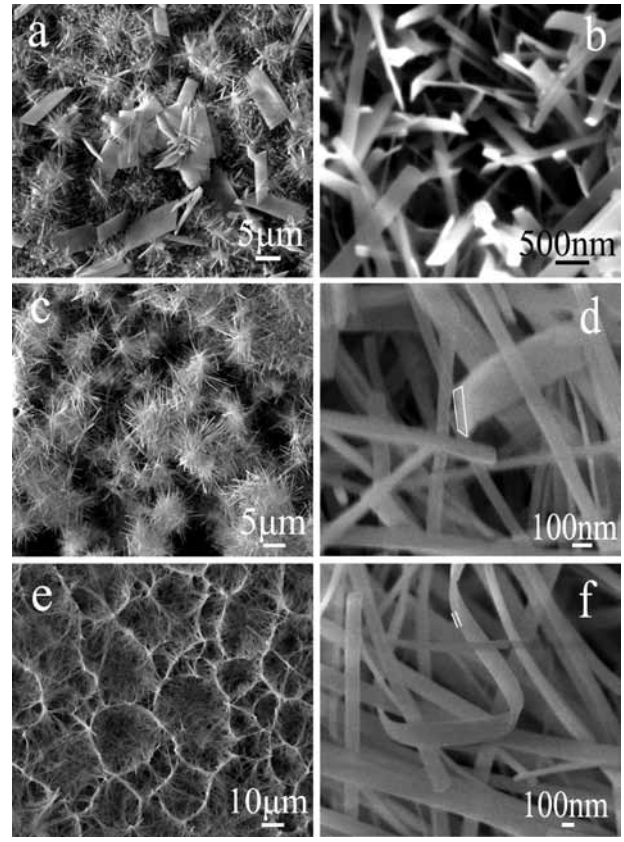

Figure 1. SEM images of the precursors prepared by adjusting the KBH_4/Se molar ratio in the Zn−Se−KBH_4−en solvothermal system: (a and b) 0:1, (c and d) 0.75:1, (e and f) 1.5:1.

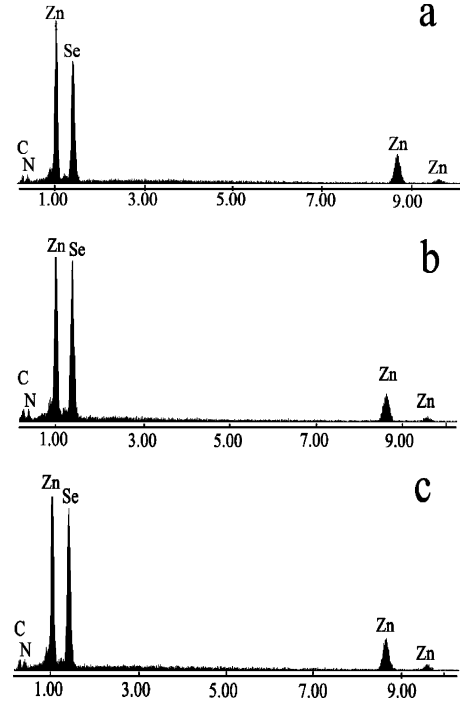

Figure 2. EDS spectra of the precursors prepared by adjusting the KBH_4/Se molar ratio in the Zn−Se−KBH_4−en solvothermal system: (a) 0:1, (b) 0.75:1, (c) 1.5:1.

(9) (a) Zhai, T. Y.; Zhong, H. Z.; Gu, Z. J.; Peng, A. D.; Fu, H. B.; Ma, Y.; Li, Y. F.; Yao, J. N. *J. Phys. Chem. C* **2007**, *111*, 2980. (b) Hu, Z. D.; Duan, F. X.; Gao, M.; Chen, Q.; Peng, L. M. *J. Phys. Chem. C* **2007**, *111*, 2987. (c) Jiang, Y.; Meng, X. M.; Yiu, W. C.; Liu, J.; Ding, J. X.; Lee, C. S.; Lee, S. T. *J. Phys. Chem. B* **2004**, *108*, 2784.
(10) Fu, H. Z.; Li, H. Y.; Jie, W. Q.; Yang, L. *J. Cryst. Growth* **2006**, *289*, 440.
(11) (a) Colli, A.; Hofmann, S.; Ferrari, A. C.; Ducati, C.; Martelli, F.; Rubini, S.; Franciosi, A.; Robertson, J. *Appl. Phys. Lett.* **2005**, *86*, 153103. (b) Hu, J. Q.; Bando, Y. S.; Zhan, J. H.; Liu, Z. W.; Golberg, D.; Ringer, S. P. *Adv. Mater.* **2005**, *17*, 975.
(12) (a) Deng, Z. X.; Wang, C.; Sun, X. M.; Li, Y. D. *Inorg. Chem.* **2002**, *41*, 869. (b) Chen, M. H.; Gao, L. *Mater. Chem. Phys.* **2005**, *91*, 437.
(13) Peng, Q.; Dong, Y. J.; Li, Y. D. *Angew. Chem., Int. Ed.* **2003**, *42*, 3027.
(14) Du, J.; Xu, L. Q.; Zou, G. F.; Chai, L. L.; Qian, Y. T. *Mater. Chem. Phys.* **2007**, *103*, 441.
(15) Xu, L.; Su, Y.; Li, S.; Chen, Y. Q.; Zhou, Q. T.; Yin, S.; Feng, Y. *J. Phys. Chem. B* **2007**, *111*, 760.

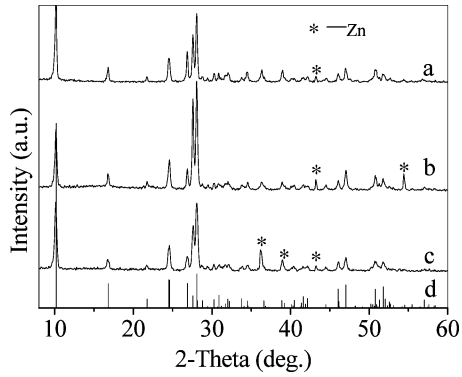

Figure 3. XRD patterns of the precursors with different morphologies prepared by adjusting the KBH_4/Se molar ratio: (a) 0:1, (b) 0.75:1, (c) 1.5:1. (d) The simulated XRD pattern from the Rietveld refinement and positional parameters of $ZnSe(en)_{0.5}$ reported by Li and co-workers.[18]

In a typical synthesis, 20 mL of en was put into a Teflon-lined autoclave of 50 mL capacity. A piece of zinc foil (1×1.5 cm^2), 0.02 g (0.25 mmol) of selenium powder, and 0−0.02 g (0−0.37 mmol) of KBH_4 were added into the autoclave. The autoclave was sealed, heated at 200 °C for 24 h, and then allowed to cool to room temperature naturally. The zinc foil covered with reaction products was removed from the solution, rinsed with deionized water and absolute ethanol two to three times, and then dried at 50 °C in an electric oven; a white-colored layer was formed on the surface of the zinc foil. The as-prepared precursors were heated to 300 °C at a rate of 30 °C/h and maintained there for 1 h in Ar in a horizontal furnace, and then a green layer was formed on the surface of the zinc foil, which was used for further analysis and characterization.

The as-prepared products were characterized by X-ray diffraction (XRD), scanning electron microscopy (SEM), high-resolution transmission electron microscopy (HRTEM), thermogravimetric analysis (TGA), and infrared (IR) and X-ray photoelectron (XPS) spectroscopy. The XRD analysis was performed using a Rigaku D/MAX-IIIC X-ray diffractometer with Cu Kα radiation (λ = 1.540598 Å) at 40 kV and 40 mA. The 2θ range used was from 5 to 70° with a speed of 8°/min. SEM images were obtained on an FEI Quanta 200 scanning electron microscope at an accelerating voltage of 20 kV. An energy-dispersive X-ray spectroscopy (EDS) system attached to the SEM was employed to analyze the chemical composition. TEM and electron diffraction images were obtained on a JEOL JEM-3010 transmission electron microscope at an accelerating voltage of 300 kV. The samples for TEM were prepared by dispersing a powdered product on a carbon-coated copper grid. The IR spectrum was recorded using a Bruker Equinx55 Fourier transform IR spectrophotometer at room temperature. TGA was carried out at a heating rate of 20 °C/min under a constant flow of N_2 gas at a rate of 100 mL/min using a TA Q600 system. XPS measurements were performed by using a Kratos Axis ultra X-ray photoelectron spectrometer with an excitation source of $Al_{K\alpha}$ = 1486.7 eV. Electrical and photosensitive properties of ZnSe ultralong nanobelts were recorded by a Keithley 2601 source measurement unit at room temperature in ambient air. A hand-held UV lamp (8 W, 254 nm) was fixed approximately 5 cm away from the sample.

3. Results and Discussion

Figure 1 shows the SEM images of these precursors in various geometrical morphologies prepared by adjusting the KBH_4/Se molar ratio in the Zn−Se−KBH_4−en solvothermal system. The products obtained in the absence of KBH_4 are composed of a large quantity of sheetlike and beltlike structures (Figure 1a and b). The lengths and widths of these sheetlike structures are in the range of 10−15 μm and 3−7 μm, respectively. These nanobelts have widths in the range of about 150−350 nm and lengths of about 2−5 μm. The length-to-width ratios of the nanostructures increase with an increase in the KBH_4/Se molar ratio, and thus the sheetlike structures were transformed into beltlike structures and ultralong nanobelts. When the KBH_4/Se molar ratio equals 0.75:1, the geometrical shape of the products is a belt (Figure 1c and d). Each nanobelt has a uniform width along its entire length; the typical lengths are in the range of 2−10 μm, and the length-to-width ratio of the nanobelts is increased to about 150. When the KBH_4/Se molar ratio is increased to 1.5:1, the products are honeycomb-like superstructures, and the entire structure is built from numerous ultralong nanobelts (Figure 1e and f). The lengths of these ultralong nanobelts are in the range of 50−100 μm and their length-to-width ratio is increased to about 660. The chemical compositions of these precursors in various geometrical morphologies were measured by the EDS system attached to the SEM. The EDS spectra are shown in Figure 2, in which C, N, Se, and Zn elements are marked. So, these precursors in various geometrical morphologies consist of C, N, Se, Zn, and H elements. Hydrogen cannot be evidenced by EDS due to its low atomic number.

The XRD patterns of these precursors in various geometrical morphologies obtained by adjusting the KBH_4/Se molar ratio were measured, and the results are shown in Figure 3. The strong and sharp diffraction peaks related to these precursors in various geometrical morphologies reveal that they are well crystallized. The positions of the diffraction peaks for these precursors are almost the same, implying that these precursors may have a similar structure. These XRD patterns were indexed by the VBTreor90 method using the PowderX program.[16] In order to avoid the interference of the Zn substrate, the 2θ values of diffraction peaks in the angular range of 5−30° in 2θ were used as input data. The results are compared, and the most reliable ones are listed in Table 1, which give consistent orthorhombic lattices with good figures of merit (FOM, M_N, and F_N, simplified criteria for the reliability of a powder diffraction indexing[17]). The indexed constants of these precursors in various geometrical morphologies are almost identical and are consistent with the values of $ZnSe(en)_{0.5}$ reported by Li et al.[18] and Lu[19] et al. Moreover, the XRD patterns match the simulated powder XRD pattern (Figure 3d) from the Rietveld refinement and positional parameters of $ZnSe(en)_{0.5}$ reported by Li et al.[18] Therefore, it is reasonable to conclude that these precursors with different morphologies may be orthorhombic $ZnSe(en)_{0.5}$

(16) (a) Dong, C. *J. Appl. Crystallogr.* **1999**, *32*, 838. (b) Dong, C.; Wu, F.; Chen, H. *J. Appl. Crystallogr.* **1999**, *32*, 850. (c) Dong, C.; Chen, H.; Wu, F. *J. Appl. Crystallogr.* **1999**, *32*, 168.
(17) (a) De Wolff, P. M. *J. Appl. Crystallogr.* **1968**, *1*, 108. (b) De Wolff, P. M. *J. Appl. Crystallogr.* **1972**, *5*, 243. (c) Smith, G. S.; Snyder, R. L. *J. Appl. Crystallogr.* **1979**, *12*, 60.
(18) Huang, X. Y.; Heulings, H. R., IV; Le, V. N.; Li, J. *Chem. Mater.* **2001**, *13*, 3754.
(19) Lu, J.; Wei, S.; Peng, Y. Y.; Yu, W. C.; Qian, Y. T. *J. Phys. Chem. B* **2003**, *107*, 3427.

Table 1. Indexing Results of XRD Patterns of the Precursors with Different Morphologies Prepared by Adjusting the KBH_4/Se Molar Ratio

precursors with different morphologies	cryst syst	*a* (Å)	*b* (Å)	*c* (Å)	vol (Å^3)	FOM
nanosheets	ortho	6.6411(0)	6.4793(4)	17.3523(0)	746.67	M_9 = 38 F_9 = 37
nanobelts	ortho	6.6513(7)	6.4787(9)	17.4200(7)	750.68	M_9 = 16 F_9 = 15
ultralong nanobelts	ortho	6.6375(1)	6.4738(4)	17.5199(7)	752.84	M_9 = 26 F_9 = 23
values of $ZnSe(en)_{0.5}$ reported by Li et al.[18]	ortho	6.6298(9)	6.4608(9)	17.350(2)	744.0(2)	

(a ZnSe−en hybrid compound). In order to further ascertain the chemical compositions of these precursors, IR spectra and TGAs of the precursors obtained in the absence of KBH_4 were performed, and the results are shown in Figures 4 and 5. In the IR spectrum shown in Figure 4, the two sharp peaks at 3236 and 3115 cm^{-1} are assigned to the $-NH_2$ asymmetric and symmetric stretching vibrations, respectively; the bands at 1580 and 1021 cm^{-1} are attributed to the $-NH_2$ scissors and wagging vibrations,[20] respectively; the absorption bands at 1355, 2933, and 2869 cm^{-1} correspond to wagging, asymmetric, and symmetric stretching vibrations of the $-CH_2$,[21] respectively; the absorption band at 1086 cm^{-1} can be assigned to the C−N stretching vibrations. The $-NH_2$ asymmetric and symmetric stretching vibrations shift toward a lower frequency, compared with that of en, because of the chemical bonding action between the Zn and N atoms. The results are consistent with that of $ZnSe(en)_{0.5}$ presented by Li and co-workers.[12a] The results suggest that en has been intercalated into these precursors. TGA results are given in Figure 5. The TGA curve shows that the precursors undergo a single-step weight-loss process and are thermally stable up to 250 °C. The measured weight loss of the en is 17.8%, which is close to the expected value of 17.2% calculated for the change of $ZnSe(en)_{0.5}$ to ZnSe. The TGA agrees with that of Li and co-workers.[18] These experimental results reveal that Zn reacts with Se and en at 200 °C for 24 h to form a ZnSe−en hybrid compound, $ZnSe(en)_{0.5}$. The $ZnSe(en)_{0.5}$ products have high crystallinity, and their geometrical shape is a sheet. The shape of the products can be changed by adding KBH_4 to the Zn−Se−en solvothermal system. The $ZnSe(en)_{0.5}$ nanosheets are transformed into $ZnSe(en)_{0.5}$ nanobelts and ultralong nanobelt arrays with honeycomb-like micropatterns with an increase in the KBH_4/Se molar ratio in the solvothermal system.

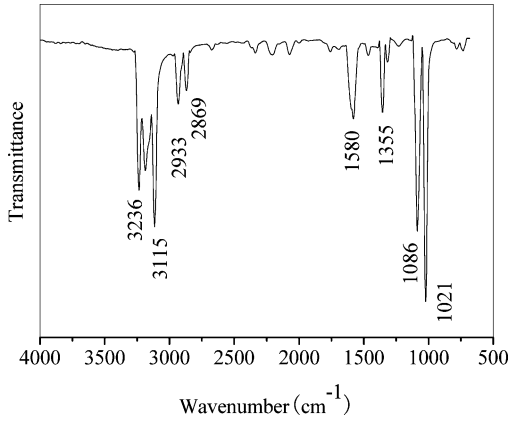

Figure 4. The IR spectrum of the precursors obtained in the absence of KBH_4.

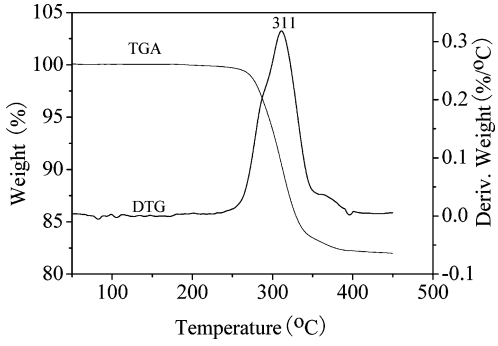

Figure 5. Thermogravimetric analysis data showing weight loss of the precursors obtained in the absence of KBH_4. The negative of the first derivative (%/°C) is also plotted as a function of the temperature.

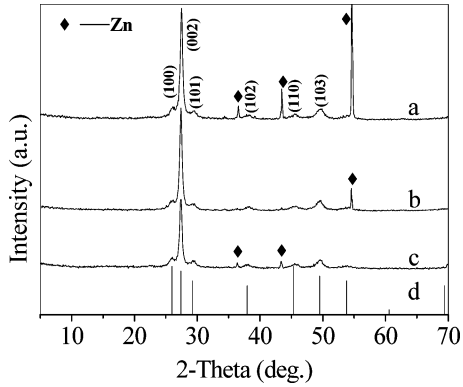

Figure 6. XRD patterns of the products after annealing the precursors prepared by adjusting the KBH_4/Se molar ratio: (a) 0:1, (b) 0.75:1, (c) 1.5:1. (d) Standard XRD pattern for ZnSe powders from the Joint Committee on Power Diffraction Standards, JPCDS card file (no. 15-0105).

The products obtained by annealing the as-synthesized $ZnSe(en)_{0.5}$ precursors in various geometrical morphologies at 300 °C for 1 h in an Ar atmosphere were characterized by XRD, SEM, and TEM; the results are shown in Figure 6−8. Figure 6 shows the XRD patterns of the annealed products. The six peaks at 2θ = 26.0, 27.4, 29.4, 38.0, 45.5, and 49.7° are observed in Figure 6. According to JCPDS card number 15-0105, the products are hexagonal wurtzite ZnSe, and these peaks are assigned to (100), (002), (101), (102), (110), and (103) diffraction lines of the hexagonal wurtzite ZnSe phase, respectively. In addition to diffraction lines of ZnSe, the diffraction lines of Zn metal from the substrate are also observed. Furthermore, the relative intensities of these peaks are distinct from those of the standard ZnSe powders (the standard diffraction of hexagonal wurtzite ZnSe powders is given in Figure 6).

(20) Mizushima, S.; Nakangwa, I.; Sweeny, D. M. *J. Chem. Phys.* **1956**, *25*, 1006.
(21) Allen, A. D.; Senoff, C. V. *Can. J. Chem.* **1965**, *43*, 888.

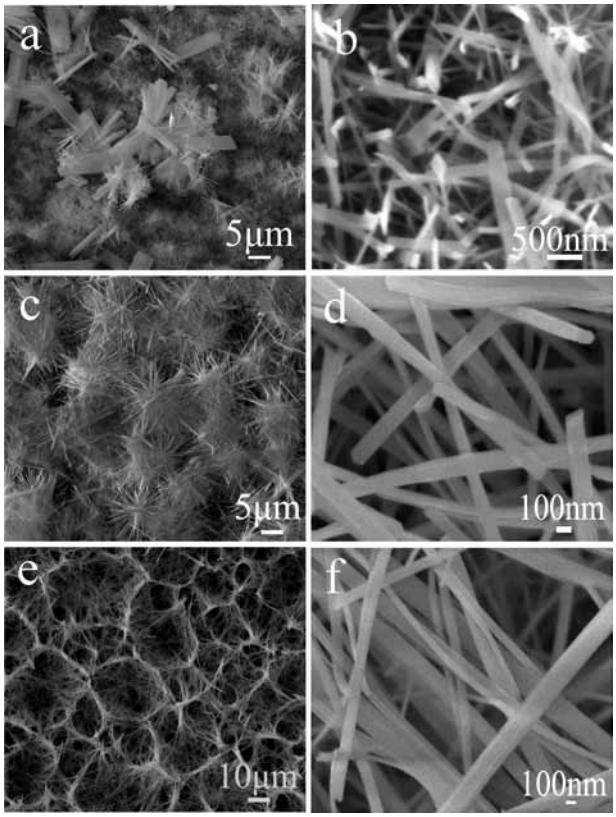

Figure 7. SEM images of the products after annealing the precursors prepared by adjusting the KBH_4/Se molar ratio: (a and b) 0:1, (c and d) 0.75:1, (e and f) 1.5:1.

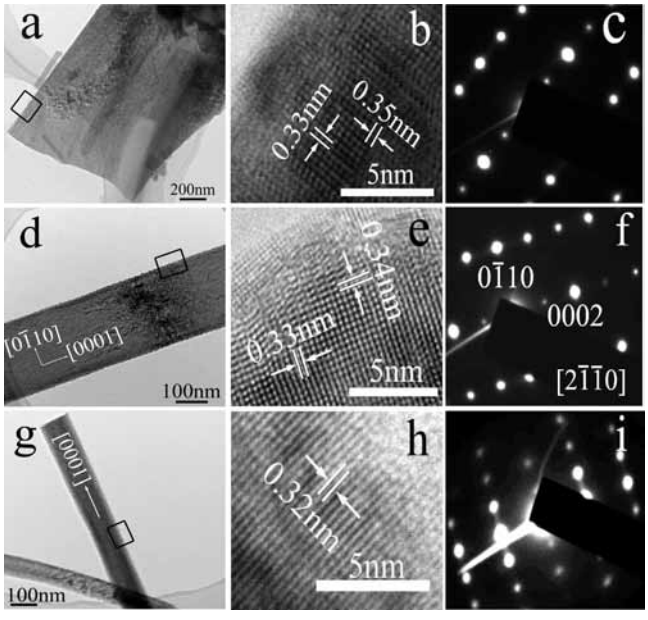

Figure 8. TEM and HRTEM images and SAED patterns of nanosheets (a−c), nanobelts (d−f), and ultralong nanobelts (g−i) of ZnSe.

The diffraction intensity of the (002) surpasses others, which illustrates that the ZnSe on the substrate has a significantly preferred orientation in the direction of [0001]. The SEM images of the annealed products are displayed in Figure 7. As can be seen in Figure 7, when $ZnSe(en)_{0.5}$ was decomposed to form ZnSe, geometrical morphologies of the nanosheets, nanobelts, and ultralong nanobelt arrays with honeycomb-like micropatterns are

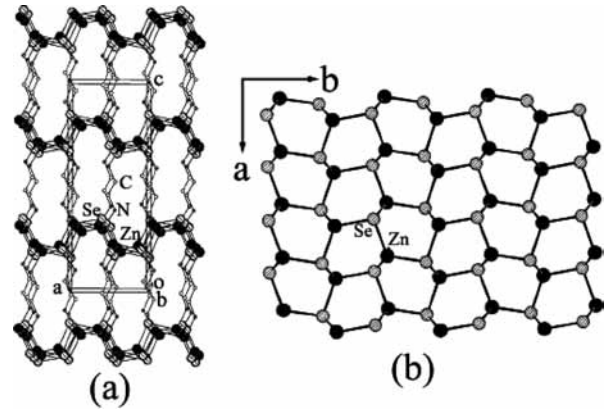

Figure 9. (a) View of $ZnSe(en)_{0.5}$ shown along the *b* axis with the unit cell outlined. The large solid circles are Zn; shaded circles are Se, and small open and shaded circles are C and N, respectively. (b) 2D [ZnSe] slab projected along the *c* axis (the figure is adapted from ref 18).

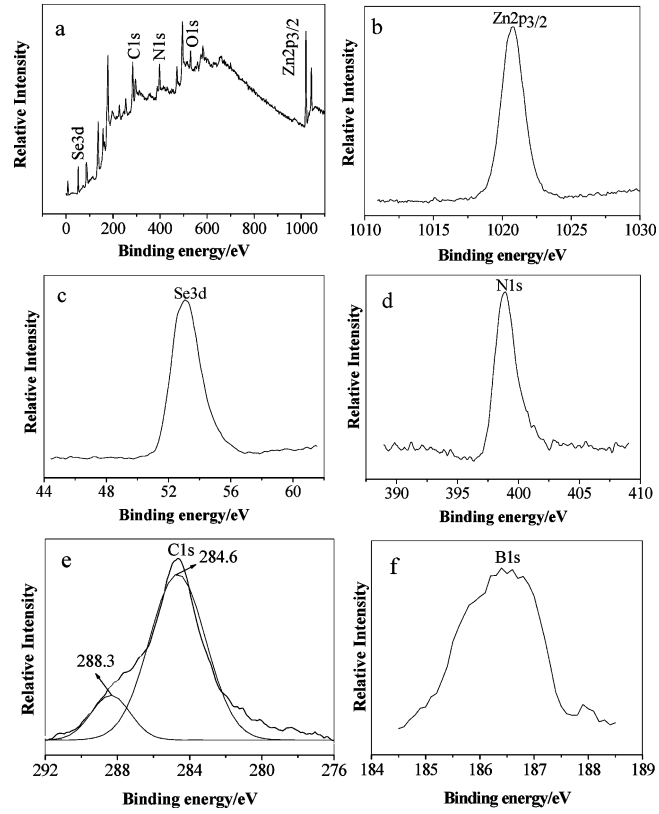

Figure 10. XPS spectra of the $ZnSe(en)_{0.5}$ ultralong nanobelt arrays with honeycomb-like micropatterns prepared in the solvothermal system with KBH_4/Se = 1.5:1.

well preserved. Figure 8 shows the TEM and HRTEM images and the corresponding selected-area electron diffraction (SAED) patterns of nanosheets, nanobelts, and ultralong nanobelt arrays with honeycomb-like micropatterns of ZnSe prepared by adjusting the KBH_4/Se molar ratio. The TEM images display the characteristic shape of the ZnSe nanosheets and nanobelts (Figure 8a,d,g). Each nanosheet or nanobelt is uniform in width and thickness, and the typical width of ZnSe nanosheets or nanobelts is 1100, 230, 110, and 75 nm as the KBH_4/Se molar ratio is 0:1, 0.75:1, and 1.5:1, respectively. Figure 8b,e,h show HRTEM images from rectangles inparts a, d, and g, respectively. As shown in HRTEM images, the

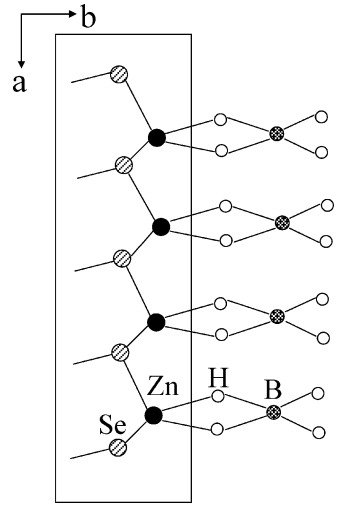

Figure 11. The structure of the BH_4^- attached to the 2D ZnSe monolayer in a bidentate fashion. The solid circles are Zn; large shaded circles are Se; open circles are H, and small shaded circles are B.

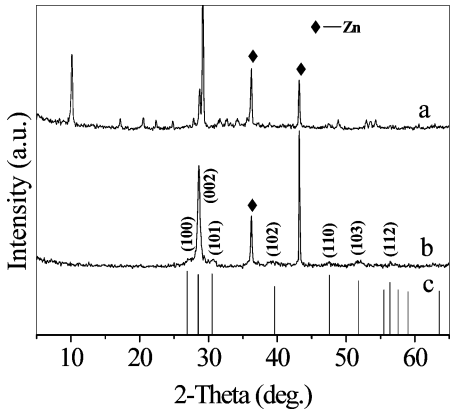

Figure 12. XRD patterns of (a) the precursors prepared in the solvothermal system with a KBH_4/thiourea molar ratio = 3:1 and (b) the annealed products. (c) Standard XRD pattern for ZnS powders from the Joint Committee on Power Diffraction Standards, JPCDS card file (no. 36-1450).

fringe spacings of the observed lattice planes are about 0.33/0.32 and 0.35/0.34 nm, respectively, which agree with the (002) and (010) lattice planes of the hexagonal ZnSe, respectively. Figure 8c,f,i show SAED images from rectangles in parts a, d, and g, respectively, and they can be indexed as the $[2\bar{1}\bar{1}0]$ zone axis of single-crystalline ZnSe with a hexagonal structure. The HRTEM and SAED show that ZnSe nanosheets and nanobelts are structurally uniform and well-crystallized single crystals. They grow along [0001] and are enclosed by $\pm(2\bar{1}\bar{1}0)$ and $\pm(01\bar{1}0)$ crystallographic facets as the top and bottom and side surfaces, respectively.

The above experimental results indicate that $ZnSe(en)_{0.5}$ nanosheets and nanobelts are synthesized by a solvothermal reaction of Zn with Se and en at 200 °C for 24 h in the absence of KBH_4 and can be transformed into ZnSe nanosheets and nanobelts by calcining in an Ar gas atmosphere at 300 °C. In our case, the Zn foil serves as both a substrate and a zinc source. The metallic zinc was easily oxidized by elemental Se because of the strong coordinating effect of en ($\log \beta[Zn(en)_2]^{2+} = 10.83$) and reacted with Se and en at 200 °C to form $ZnSe(en)_{0.5}$, which was decomposed to form ZnSe. The chemical reactions can be formulated as follows:

$$Zn + Se + 0.5en \rightarrow ZnSe(en)_{0.5} \quad (1)$$

$$ZnSe(en)_{0.5} \rightarrow ZnSe + 0.5en \quad (2)$$

According to Li et al.[18] and Lu et al.,[19] the crystal structure of $ZnSe(en)_{0.5}$ is a three-dimensional network containing monolayers of ZnSe slabs that are interconnected by bridging en molecules. The coordination of Zn^{2+} in $ZnSe(en)_{0.5}$ is similar to the $ZnSe_4$ tetrahedra in hexagonal ZnSe. Figure 9a illustrates a view of $ZnSe(en)_{0.5}$ along the *b* axis, where the $ZnNSe_3$ coordination tetrahedra are revealed. The ZnSe slab is a puckered 6^3 net formed by alternating three-coordinated Zn and Se (Figure 9b). It can be regarded as a "slice" cut from the wurtzite-type structure of ZnSe. The interconnections between any two adjacent slabs are made by en molecules bridged to two metal atoms from the two slabs. For $ZnSe(en)_{0.5}$, $ZnS(en)_{0.5}$, and so forth inorganic−organic hybrid composites, there are two preferential growth directions, [0001] and $[0\bar{1}10]$;[22] thus, the sheet- and beltlike nanostructures are produced. When en molecules are removed from $ZnSe(en)_{0.5}$ by annealing at 300 °C in Ar, Zn−N bonds are broken, 2D [ZnSe] monolayers collapse along the *c* axis, and the fourth Zn−Se bonds form, which results in hexagonal ZnSe crystallites. In addition, the length-to-width ratio of the nanostructures was evidently increased when KBH_4 was added into the Zn−Se−en solvothermal system.

In order to illuminate the role of KBH_4 in the control over the $ZnSe(en)_{0.5}$ nanostructures with different morphologies, the $ZnSe(en)_{0.5}$ ultralong nanobelt arrays with honeycomb-like micropatterns prepared in the solvothermal system with KBH_4/Se = 1.5:1 were characterized and analyzed by atomic emission spectroscopy and XPS. The analytical result of atomic emission spectroscopy indicates that the products contain Zn, Se, and B elements. The XPS spectra are shown in Figure 10, including (a) the survey spectrum, (b) $Zn2p_{3/2}$, (c) Se3d, (d) N1s, (e) C1s, and (f) B1s. The binding energies obtained in the XPS analysis were corrected for specimen charging through referencing the C1s to 284.6 eV. The O peak might come from H_2O and O_2 absorbed on the surface of the sample in air. The binding energy of $Zn2p_{3/2}$ is identified at 1021 eV (Figure 10b). The peak at about 53.1 eV corresponds to Se3d, which is derived from $ZnSe(en)_{0.5}$ (Figure 10c). The signal at about 398.9 eV can be attributed to N1s (Figure 10d), which is derived from en in $ZnSe(en)_{0.5}$. The peaks at about 284.6 and 288.3 eV can be attributed to C1s (Figure 10e), which are derived from contamination carbon and en in $ZnSe(en)_{0.5}$, respectively. The weak peak at about 186.5 eV can be assigned to B1s (Figure 10f), which might come from BH_4^- absorbed on the surface of the $ZnSe(en)_{0.5}$ ultralong nanobelts. Moreover, $NaBH_4$ was used as a substitute for KBH_4, $ZnSe(en)_{0.5}$ nanobelts and ultralong nanobelts were also obtained. The anisotropic growth of the 1D nanostructure is often driven by using capping ligands

(22) Lu, F.; Cai, W. P.; Zhang, Y. G.; Li, Y.; Sun, F. Q.; Heo, S. H.; Cho, S. O. *J. Phys. Chem. C* **2007**, *111*, 13385.

Table 2. Indexing Results of the XRD Pattern of the ZnS Precursors Prepared in the Zn−Thiourea−KBH_4−en Solvothermal System with a KBH_4/Thiourea Molar Ratio = 3:1

	cryst syst	*a* (Å)	*b* (Å)	*c* (Å)	vol (Å^3)	FOM
ZnS precursors	ortho	17.2672(8)	6.3688(7)	6.1847(5)	680.16	M_{12} =19 F_{12} = 18
values of $ZnS(en)_{0.5}$ reported by Ouyang[28]	ortho	17.263(1)	6.393(1)	6.205(1)	684.78(1)	

that could bind selectively onto particular facets of the seed particles.[23,24] It is well-known that KBH_4 is a strong reducing agent; however, the tetrahydroborate ion, BH_4^- has a tendency to form unusual covalent complexes with transition metals. The ligation is invariably through bridging hydrogen atoms.[25] Therefore, it is reasonable to conclude that, when KBH_4 is introduced into the solvothermal system, BH_4^- may serve as a ligand to Zn and adsorb on the Zn facets perpendicular to the *b* axis of the $ZnSe(en)_{0.5}$ nuclei. The most likely structure is shown in Figure 11. The tetrahedral BH_4^- ligands are attached to the Zn facets in a bidentate fashion. The presence of BH_4^- suppresses the growth of the $ZnSe(en)_{0.5}$ nuclei along the *b* axis, and thus the $ZnSe(en)_{0.5}$ nanobelts are obtained. With increasing the KBH_4/Se molar ratio, the growth along the *b* axis is further suppressed, and ultralong nanobelts are obtained. These ultralong nanobelts self-assembled into honeycomb-like micropatterns due to capillary forces.[26,27]

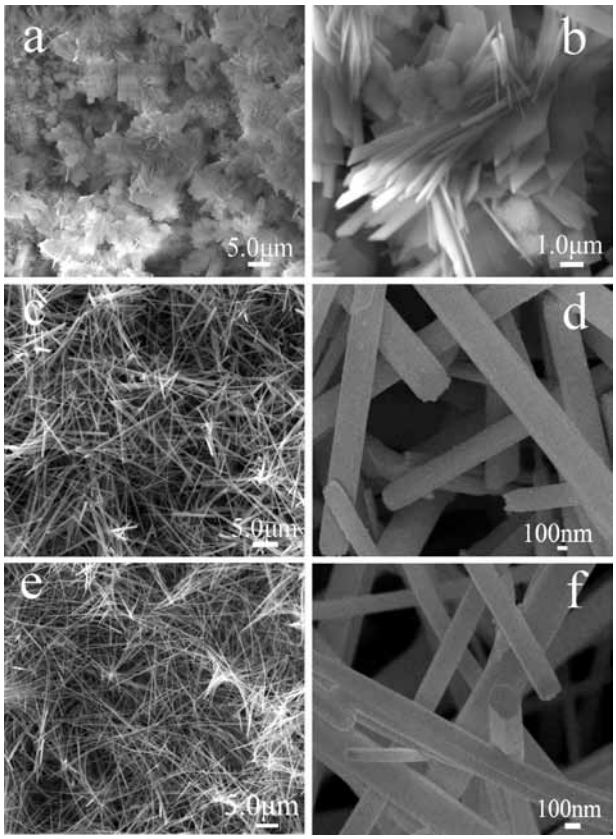

Figure 13. SEM images of the ZnS samples prepared by adjusting the KBH_4/thiourea molar ratio in the solvothermal system and subsequent annealing: (a and b) 0:1, (c and d) 1.5:1, (e and f) 3:1.

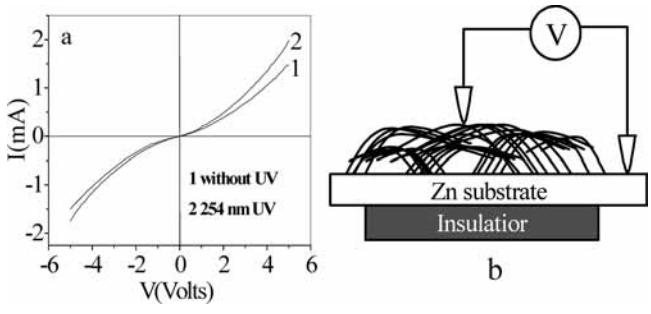

Figure 14. (a) I−V curves of ZnSe ultralong nanobelt arrays with honeycomb-like micropatterns. (b) The schematic diagram of the current sensing measurement.

In addition, controllable syntheses of ZnS nanosheets and nanowires with various aspect ratios were also achieved by adjusting the KBH_4/thiourea molar ratio in the Zn−thiourea−KBH_4−en solvothermal system and subsequent annealing. The precursors prepared by adjusting the KBH_4/thiourea molar ratio at 200 °C for 24 h and the products obtained by annealing the precursors at 300 °C in Ar were characterized by XRD and SEM. The XRD patterns of the precursors prepared in the solvothermal system with the KBH_4/thiourea molar ratio = 3:1 and the annealed products are shown in Figure 12, in which the standard diffraction of hexagonal wurtzite ZnS powders is also given (sticks in Figure 12). The XRD pattern of the precursors (Figure 12a) was indexed by the VBTreor90 method using the PowderX program. The results are listed in Table 2. It can be seen that the indexed constants are consistent with that of $ZnS(en)_{0.5}$ reported by Ouyang et al.[28] Therefore, the precursors may be orthorhombic $ZnS(en)_{0.5}$. The XRD pattern of the annealed products illustrates that the annealed products are hexagonal wurtzite ZnS, and the ZnS on the substrate has significantly preferred orientation in the direction of [0001]. Figure 13 shows SEM images of the ZnS samples prepared by adjusting the KBH_4/thiourea molar ratio in the solvothermal system and subsequent annealing. The geometrical shape of ZnS obtained in the absence of KBH_4 is a sheetlike structure (Figure 13a and b). The lengths and widths of these sheetlike structures are in the range of 5−10 μm and 0.5−2.5 μm, respectively. The length-to-width ratios of the ZnS nanostructures increase with an increase in the KBH_4/thiourea molar ratio, and thus the sheetlike structures are transformed into wirelike structures. When the KBH_4/thiourea molar ratio equals 1.5:1 and 3:1, the length-to-width ratios of the nanowires are increased to 150 and 500, respectively.

(23) Xiong, S. L.; Xi, B. J.; Wang, C. M.; Xi, G. C.; Liu, X. Y.; Qian, Y. T. *Chem. Eur. J.* **2007**, *13*, 7926.
(24) Greene, L. E.; Yuhas, B. D.; Law, M.; Zitoun, D.; Yang, P. D. *Inorg. Chem.* **2006**, *45*, 7535.
(25) Marks, T. J.; Kolb, J. R. *Chem. Rev.* **1977**, *77*, 263.
(26) Liu, H.; Li, S. H.; Zhai, J.; Li, H. J.; Zheng, Q. S.; Jiang, L.; Zhu, D. B. *Angew.Chem. Int. Ed.* **2004**, *43*, 1146.
(27) Lu, C. H.; Qi, L. M.; Yang, J. H.; Tang, L.; Zhang, D. Y.; Ma, J. M. *Chem. Commun.* **2006**, *33*, 3551.
(28) Ouyang, X.; Tsai, T. Y.; Chen, D. H.; Huang, Q. J.; Cheng, W. H.; Clearfield, A. *Chem. Commun.* **2003**, 886.

Figure 14a shows the current−voltage (I−V) curves of ZnSe ultralong nanobelt arrays with honeycomb-like micropatterns measured in the dark and upon UV-light exposure. Figure 14b is the schematic diagram of the current-sensing measurement. We notice that the UV-exposed ZnSe nanobelts have a lower resistivity; both I−V curves exhibit nonlinear behavior and are similar to those observed from the ZnSe[29] and Si[30] nanowires. The superlinear characteristics can be explained by reference to concentration fluctuations along the nanobelt length.[29]

4. Conclusion

In summary, we have developed a novel solvothermal route to prepare single-crystalline ZnSe nanosheets and nanobelts with various length-to-width ratios. The length-to-width ratio can be adjusted in the range of 1.5−660 by changing the amount of KBH_4 in the Zn−Se−KBH_4−en solvothermal system. In addition, variable-aspect ratio ZnS nanosheets and nanowires were also synthesized by adjusting the KBH_4/thiourea molar ratio in the Zn−thiourea−KBH_4−ethylenediamine solvothermal system. It can be expected that a controllable synthesis of other II−VI semiconductor nanostructures can be achieved by a method similar to that from organic−inorganic hybird precursors containing II−VI slabs such as $ZnTe(en)_{0.5}$, $MnS(en)_{0.5}$, $NiS(en)_{0.5}$, and so forth. The method may provide opportunities for both fundamental research and technological applications.

Acknowledgment. We thank the National Natural Science Foundation of China (Grant No. 20573072) and Specialized Research Fund for the Doctoral Program of Higher Education (Grant No. 20060718010) for support of this work.

IC801054E

(29) Philipose, U.; Ruda, H. E.; Shik, A.; De Souza, C. F.; Sun, P. *J. Appl. Phys.* **2006**, *99*, 066106.
(30) Cui, Y.; Duan, X. F.; Hu, J. T.; Lieber, C. M. *J. Phys. Chem. B* **2000**, *104*, 5213.